

Article

# Shape Memory Polymer Composites of Poly(styrene-*b*-butadiene-*b*-styrene) Copolymer/Liner Low Density Polyethylene/Fe<sub>3</sub>O<sub>4</sub> Nanoparticles for Remote Activation

Yongkun Wang \*, Junjie Ye and Wenchao Tian

Key Laboratory of Ministry of Education for Electronic Equipment Structure Design, Xidian University, Xi'an 710071, China; jjye@xidian.edu.cn (J.Y.); wctian@xidian.edu.cn (W.T.)

\* Correspondence: ykwang@xidian.edu.cn; Tel.: +86-29-8820-2954

Academic Editor: Jiazhao Wang

Received: 14 October 2016; Accepted: 28 October 2016; Published: 3 November 2016

**Abstract:** Magnetically sensitive shape memory poly(styrene-*b*-butadiene-*b*-styrene) copolymer (SBS)/liner low density polyethylene (LLDPE) composites filled with various contents of Fe<sub>3</sub>O<sub>4</sub> nanoparticles were prepared. The influence of the Fe<sub>3</sub>O<sub>4</sub> nanoparticles content on the thermal properties, mechanical properties, fracture morphology, magnetic behavior, and shape memory effect of SBS/LLDPE/Fe<sub>3</sub>O<sub>4</sub> composites was systematically studied in this paper. The results indicated that homogeneously dispersed Fe<sub>3</sub>O<sub>4</sub> nanoparticles ensured the uniform heat generation and transfer in the alternating magnetic field, and endowed the SBS/LLDPE/Fe<sub>3</sub>O<sub>4</sub> composites with an excellent magnetically responsive shape memory effect. When the shape memory composites were in the alternating magnetic field ( $f = 60$  kHz,  $H = 21.21$  kA·m<sup>-1</sup>), the best shape recovery ratio reached 99%, the shape retention ratio reached 99.4%, and the shape recovery speed increased significantly with the increment of Fe<sub>3</sub>O<sub>4</sub> nanoparticles. It is anticipated that tagging products with this novel shape memory composite is helpful for the purpose of an intravascular delivery system in Micro-Electro-Mechanical System (MEMS) devices.

**Keywords:** SBS/LLDPE blends; Fe<sub>3</sub>O<sub>4</sub> nanoparticles; magnetic properties; shape memory effect

## 1. Introduction

Shape memory polymers (SMPs) are a kind of material that can perceive external stimuli (heat, light, electric field, magnetic field, pH, specific ions and enzymes) and make a corresponding stimulation to the appropriate stimulus [1–9]. These SMPs have attracted more and more attention due to a wide range of applications, including smart textiles and apparel, heat shrinkable packaging, intelligent biomedical materials and self-deployable structures in spacecrafts [10–14]. In the present study, the thermally activated SMPs are the most common. The basic mechanism of shape recovery can be attributed to the “shrinkage” of oriented, extended chains triggered by melting or glass transition [15]. However, the thermally activated SMPs will not be allowed for certain attractive applications where the temperature is not easy to obtain. Therefore, it is very necessary to design the remote control of SMPs. In fact, a couple of remote triggering methods, including light and an alternating magnetic field, have been developed to achieve the noncontact activation of the shape memory effect [16]. In addition, these remote-activated SMPs have attracted a great deal of interest recently. This paper is mainly focused on the magnetically sensitive SMPs.

To date, one of the immediate methods is using magnetically responsive fillers to fill the SMPs to prepare the magnetic active shape memory polymer composites. Additionally, the most commonly used nano-fillers are Fe<sub>3</sub>O<sub>4</sub> nanoparticles. Yakacki et al. [17] filled methacrylate-based thermoset

SMPs with  $\text{Fe}_3\text{O}_4$  nanoparticles (1–2.5 wt %) to prepare shape memory polymer composites for remote activation and investigated the shape memory behavior of the composites. The results showed that increasing  $\text{Fe}_3\text{O}_4$  concentrations led to the decrease of the glass transition temperature and rubbery modulus. The low crosslinking degree of networks and high magnetite concentrations showed a significant amount of irrecoverable strain. Cai et al. [18] synthesized and studied the properties of magnetically sensitive shape memory  $\text{Fe}_3\text{O}_4$ /Poly( $\epsilon$ -caprolactone)-polyurethane nanocomposites. It is shown that with increasing the content of  $\text{Fe}_3\text{O}_4$  nanoparticles, the shape memory properties of the nanocomposites in an alternating magnetic field increased and the best recovery rate reached 97%. They pointed out that this composite can be used for biomedical applications. Kokate et al. reported that poly(3,4-ethylene dioxythiophene)/ $\text{Fe}_3\text{O}_4$  composites can be useful for information storage applications [19]. They also studied the performance of the composites and found that the thermal stability and saturation magnetization of the composites increased with the increase in  $\text{Fe}_3\text{O}_4$  content.

In this paper, we synthesized the nano- $\text{Fe}_3\text{O}_4$  particles to fill the shape memory poly(styrene-*b*-butadiene-*b*-styrene) copolymer (SBS)/linear low density polyethylene (LLDPE) blends, and prepared the magnetically sensitive shape memory SBS/LLDPE/ $\text{Fe}_3\text{O}_4$  composites. The novel magnetically sensitive shape memory polymer composite is simple to fabricate and easy to design to achieve good shape memory properties. The shape memory blend consists of two components, one is SBS and other is LLDPE. The LLDPE is the most commonly used plastic and is often used in blends for balanced mechanical properties and processability. SBS has the mechanical properties of a vulcanized rubber and the processability of a thermoplastic. In addition, the nonpolar nature of the SBS plus the presence of double bonds and aromatic rings in the chains are expected to improve the interaction of the polymer with the LLDPE. Furthermore, the LLDPE acts as a reversible phase, and SBS and crosslinking networks between the SBS and LLDPE act as a fixed phase. The shape memory polymer composites were studied for their structural, micro-structural, thermal, optical and magnetic properties by using various characterization techniques.

## 2. Experimental

### 2.1. Materials

SBS (PS:PB = 30/70, YH-791) with a density of  $0.93 \text{ g/cm}^3$ ,  $M_n = 1.46 \times 10^5$  and  $M_w/M_n = 1.09$ , was purchased from Balin Petroleum Chemical Corporation, Sinopec Group, Yueyang, China. LLDPE (DGM-1820) with a density of  $0.92 \text{ g/cm}^3$  and a melt flow rate (MFR) of  $1.6 \text{ g/10 min}$  was manufactured by Tianjin Petro-Chemical Corp, Tianjin, China. Benzene (99%) and acetone (99.5%) were received from Acros (Shanghai, China). Ferric chloride ( $\text{FeCl}_3 \cdot 6\text{H}_2\text{O}$ ) and sodium acetate (NaAc) were purchased from local agent companies (Yuhua Xi'an biological science and Technology Co., Ltd., Xi'an, China). These materials were used without further purification.

### 2.2. Preparation of $\text{Fe}_3\text{O}_4$ Nanoparticles

The synthesis of magnetite nanoparticles was performed by precipitating iron salts ( $\text{FeCl}_3 \cdot 6\text{H}_2\text{O}$  and  $\text{FeSO}_4 \cdot 7\text{H}_2\text{O}$ ) in alkaline medium as reported. The detailed steps are as follows: 1.56 g  $\text{FeSO}_4 \cdot 7\text{H}_2\text{O}$  and 2.72 g  $\text{FeCl}_3 \cdot 6\text{H}_2\text{O}$  were dissolved into 120 mL deionized water in a 250 mL four-neck flask. This solution was stirred under mechanical stirring and a nitrogen atmosphere at  $80 \text{ }^\circ\text{C}$  for 10 min. The magnetic particles formed through coprecipitation of  $\text{Fe}^{2+}$  and  $\text{Fe}^{3+}$  salts by rapid addition of 17 mL NaAc. The precipitate  $\text{Fe}_3\text{O}_4$  nanoparticles were washed by repeated cycles of centrifugation and redispersion in deionized water [20,21].

### 2.3. Preparation of $\text{Fe}_3\text{O}_4$ /SBS/LLDPE Composites

SBS, LLDPE and  $\text{Fe}_3\text{O}_4$  nanoparticles were blended in a Banbury mixer (PLE 651, Brabender, Germany) at  $130 \text{ }^\circ\text{C}$  for 10 min. After blending, samples were compressed into plates at  $160 \text{ }^\circ\text{C}$  with the pressure of 10 MPa. After the curing process, the thickness of the developed composites was

approximately 2 mm. Fe<sub>3</sub>O<sub>4</sub>/SBS/LDPE composites with Fe<sub>3</sub>O<sub>4</sub> weight fractions of 4.5, 9, 13.5 and 18 wt % was fabricated in this way. For comparison, a pure SMP specimen was cured under the same conditions.

#### 2.4. Sample Irradiation

The specimens were placed in polyethylene sample bags and were irradiated at 100 kGy by 60Co  $\gamma$ -rays under vacuum ( $10^{-3}$  torr) at 20 to 30 °C at a dose rate of 1 Gy/s. The dose range of 100 kGy was selected based on our previous work [22].

#### 2.5. Experimental Methods

**Mechanical properties.** In order to investigate the influence of Fe<sub>3</sub>O<sub>4</sub> nanoparticles contents on the mechanical properties of Fe<sub>3</sub>O<sub>4</sub>/SBS/LLDPE composites, tensile tests at room temperature were performed with a SANS tester (Shenzhen SANS Material Test Instrument Co. Ltd., Shenzhen, China) according to ASTM D412. The strain rate was 2 mm·min<sup>-1</sup>.

**DSC.** To explore the influence of the Fe<sub>3</sub>O<sub>4</sub> nanoparticles contents on thermal properties, the thermal properties of the SMPs were analyzed by differential scanning calorimetry (DSC) conducted on a DSC Pyris 1 (Perkin Elmer, ltham city, MA, USA). The samples of about 5.0 mg were heated from 0 to 130 °C at a constant rate of 10 °C·min<sup>-1</sup> and then passed through a cooling cycle with the same rate, and  $T_m$ s were determined by this step.

**DMA.** A dynamic mechanical analyzer was used to obtain the storage modulus of the Fe<sub>3</sub>O<sub>4</sub>/SBS/LLDPE composites. Dynamic mechanical analysis (DMA) was carried out in tensile loading mode using a DMA Q800 (TA Instruments, New Castle, DE, USA) to determine the thermo-mechanical properties. The samples were cut to dimensions of 2 × 12 × 30 mm<sup>3</sup> and the edges of the samples were wet sanded with 600 grit sandpapers. And the single cantilever clamping fixture (TA Instruments, New Castle, DE, USA) was used with amplitude of 10  $\mu$ m, a frequency of 1 Hz. The temperature was ramped from -20 to 130 °C at a rate of 3 °C/min.

**TEM and SEM.** The particle size and morphology were characterized by the Transmission electron microscopy (TEM, Hitachi, H-600, Tokyo, Japan) and scanning electron microscope (SEM, INCA X-ACT, Tescan, Brno, Czech Republic). The Fe<sub>3</sub>O<sub>4</sub>/SBS/LLDPE composites were frozen in liquid nitrogen for 30 min, and then fractured quickly. The broken surfaces were sputter coated with a gold layer and observed with SEM.

**Shape memory properties of Fe<sub>3</sub>O<sub>4</sub>/SBS/LLDPE composites.** The shape memory properties of Fe<sub>3</sub>O<sub>4</sub>/SBS/LLDPE composites were investigated by a method called fold-deploy shape memory test [23]. According to this method, the shape memory properties could be obtained by recording the bending angle. The specimens of 50 × 10 × 2 mm<sup>3</sup> (length × width × thickness) were folded at 110 °C followed by quenching into an ice-water bath. The folded samples were reheated at 110 °C or placed into an alternating magnetic field ( $f = 60$  kHz) (GP-25 ultra-audio frequency induction heating equipment, Shannxi, China) to recover its original shape. The shape memory test of all samples was repeated for three times. The shape recovery process was recorded by using a digital camera (Canon Corporation, Tokyo, Japan). The changed angles of specimens were recorded;  $\theta_f$  was the angle of the folded samples after being exposed to room temperature for 5 min, and  $\theta_r$  was the final angle after one shape recovery process. The shape retention rate ( $R_f$ ) and shape recovery rate ( $R_r$ ) were calculated using Equations (1) and (2).

$$R_f(\%) = \frac{180^\circ - \theta_f}{180^\circ} \times 100 \quad (1)$$

$$R_r(\%) = \frac{\theta_r}{180^\circ} \times 100 \quad (2)$$

### 3. Results and Discussion

#### 3.1. Characteristics of the Fe<sub>3</sub>O<sub>4</sub> Nanoparticles

Fe<sub>3</sub>O<sub>4</sub> nanoparticles were prepared through the solvothermal method, and the morphology of Fe<sub>3</sub>O<sub>4</sub> nanoparticles was characterized by TEM and SEM. As can be seen from Figure 1, the Fe<sub>3</sub>O<sub>4</sub> nanoparticles have a spherical shape with a rough surface and a relatively uniform size of around 350 nm. The magnetic response curve of Fe<sub>3</sub>O<sub>4</sub> nanoparticles is shown in Figure 2. From the curve, it can be found that the magnetic response of prepared Fe<sub>3</sub>O<sub>4</sub> nanoparticles was 80 emu/g. This meets the requirements to prepare the magnetically controlled shape memory polymer composite.

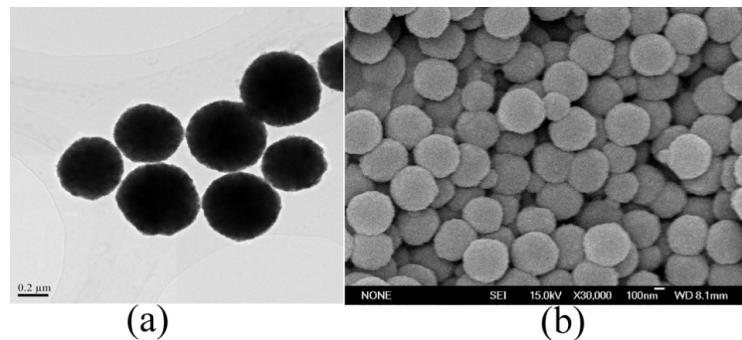


**Figure 1.** (a) Transmission electron microscope (TEM) and (b) Scanning electron microscope (SEM) images of the Fe<sub>3</sub>O<sub>4</sub> nanoparticles.

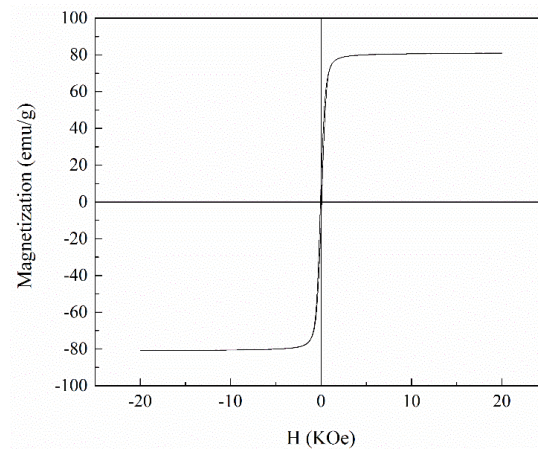


**Figure 2.** Magnetization curve of Fe<sub>3</sub>O<sub>4</sub> nanoparticles.

#### 3.2. Characteristics of the Fe<sub>3</sub>O<sub>4</sub>/SBS/LLDPE Composites

##### 3.2.1. Mechanical Properties

The relationship between the mechanical properties and the Fe<sub>3</sub>O<sub>4</sub> nanoparticle content is illustrated in Figure 3. Each sample is characterized by tensile tests conducted at room temperature. It is observed that the tensile strength of the composites increases with the increasing Fe<sub>3</sub>O<sub>4</sub> nanoparticle content. This indicates that the mechanical properties of the composites improve as the Fe<sub>3</sub>O<sub>4</sub> nanoparticles fill the bulk SMP. However, the curve slightly decreases when the Fe<sub>3</sub>O<sub>4</sub> nanoparticle content approaches 13.5 wt %, which is attributed to the beginning of the agglomeration of the Fe<sub>3</sub>O<sub>4</sub> nanoparticles. It is noted that the elongation at the break of the Fe<sub>3</sub>O<sub>4</sub>/SBS/LLDPE composites decreases significantly with the increment of the Fe<sub>3</sub>O<sub>4</sub> nanoparticles. This indicates that the toughness of the composites decreases with the Fe<sub>3</sub>O<sub>4</sub> nanoparticles increasing.

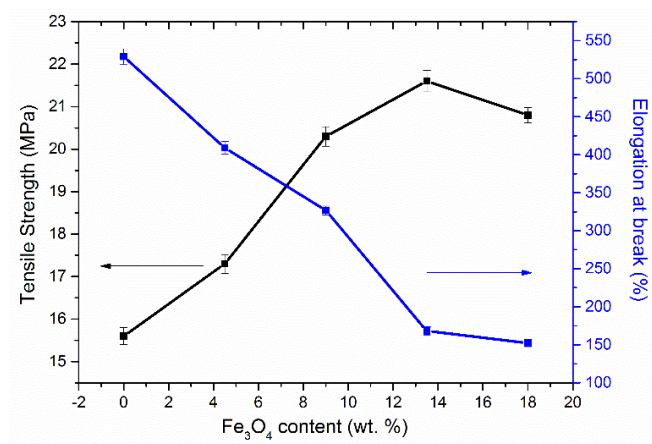


Figure 3. Mechanical properties of Fe<sub>3</sub>O<sub>4</sub>/SBS/LLDPE composites.

### 3.2.2. The SEM of Fe<sub>3</sub>O<sub>4</sub>/SBS/LLDPE Composites

To show the distribution of nanoparticles in a polymer matrix of a dry state, SEM was used to investigate the fracture surfaces. Figure 4 showed that the Fe<sub>3</sub>O<sub>4</sub> nanoparticles were uniformly dispersed in the SBS/LLDPE blends when the Fe<sub>3</sub>O<sub>4</sub> nanoparticle content was less than 13.5 wt %. However, a higher Fe<sub>3</sub>O<sub>4</sub> nanoparticle content ( $w > 13.5\%$ ) caused a serious nanoparticle aggregation, and this may be the reason for the decline of the mechanical properties of the composite, as shown in Figure 3.

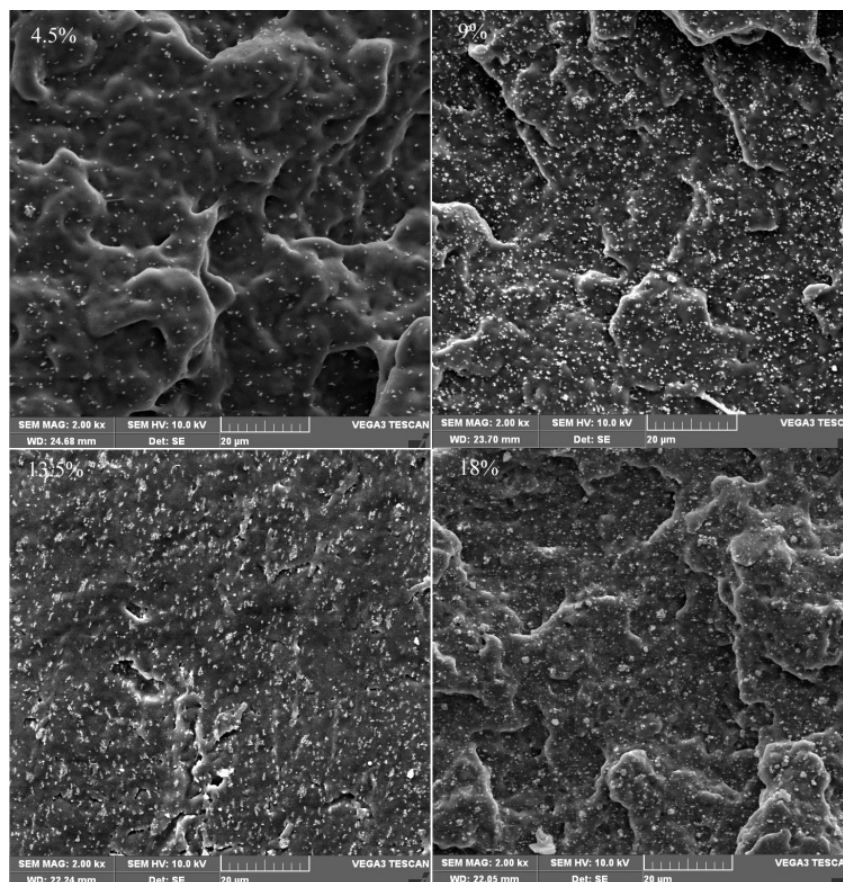
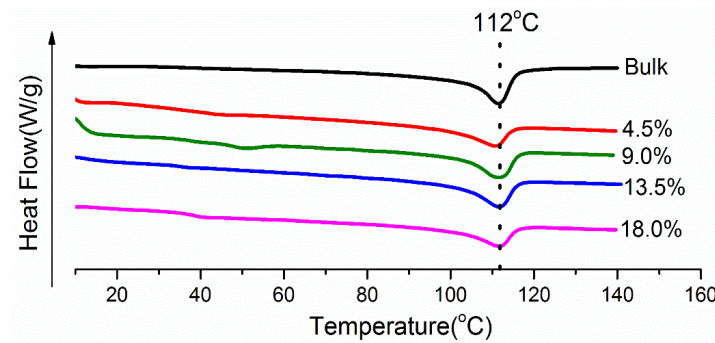


Figure 4. SEM of the Fe<sub>3</sub>O<sub>4</sub>/SBS/LLDPE composites.

### 3.2.3. Thermal Analysis of Fe<sub>3</sub>O<sub>4</sub>/SBS/LLDPE Composites

The influence of Fe<sub>3</sub>O<sub>4</sub> nanoparticle contents on the thermal properties of Fe<sub>3</sub>O<sub>4</sub>/SBS/LLDPE composites was investigated by DSC and DMA. From Figure 5, it can be found that the melting temperatures of Fe<sub>3</sub>O<sub>4</sub>/SBS/LLDPE composites were not significantly affected by the incorporation of Fe<sub>3</sub>O<sub>4</sub> nanoparticles.



**Figure 5.** Differential scanning calorimetry (DSC) curves of the Fe<sub>3</sub>O<sub>4</sub>/SBS/LLDPE composites.

Usually, a good shape memory composite should have a large change of the storage modulus ( $E'$ ) for more than two to three orders below and above the shape memory transition temperature [24]. Figure 6 illustrates that the storage moduli of the Fe<sub>3</sub>O<sub>4</sub>/SBS/LLDPE composites below the shape memory transition temperature are about two orders of magnitude larger than that above the shape memory transition temperature, which means that the Fe<sub>3</sub>O<sub>4</sub>/SBS/LLDPE composites meet the above requirements. The curves also reveal that the glassy/rubbery moduli exhibited a systematic increase with the Fe<sub>3</sub>O<sub>4</sub> nanoparticles' weight fraction. It indicates that the incorporation of Fe<sub>3</sub>O<sub>4</sub> nanoparticles reinforces the SMPs. The storage moduli of all samples decrease slowly along with temperatures increasing, and then descend abruptly when the temperature rises to about 110 °C, which is attributed to the melting of the semi-crystalline SBS/LLDPE matrix.

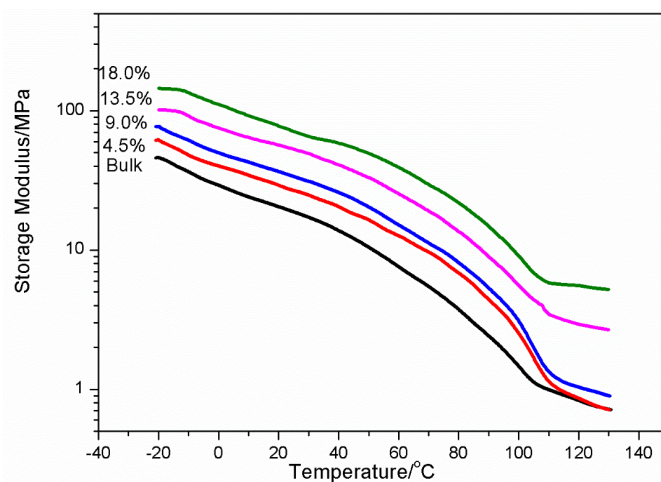


**Figure 6.** Storage modulus of the Fe<sub>3</sub>O<sub>4</sub>/SBS/LLDPE composites.

### 3.2.4. Magnetically Induced Shape Recovery of Fe<sub>3</sub>O<sub>4</sub>/SBS/LLDPE Composites

The effect of the magnetic field intensity on the shape memory of the Fe<sub>3</sub>O<sub>4</sub>/SBS/LLDPE composites was analyzed to choose the optimal magnetic field intensity. The SBS/LLDPE composite with 13.5 wt % Fe<sub>3</sub>O<sub>4</sub> nanoparticles was chosen to test the shape memory behavior of the composite in

different magnetic field intensities ( $H = 7.07, 14.14, 21.21, 28.28,$  and  $35.36 \text{ kA}\cdot\text{m}^{-1}$ ). Figure 7 indicates that in a higher-intensity magnetic field, the shape recovery time decreases drastically. However, the shape recovery time show balance when the magnetic field intensity was more than  $21.21 \text{ kA}\cdot\text{m}^{-1}$ . Thus, in this article, we studied the shape memory properties of the samples under a fixed alternating magnetic field ( $f = 60 \text{ kHz}, H = 21.21 \text{ kA}\cdot\text{m}^{-1}$ ).

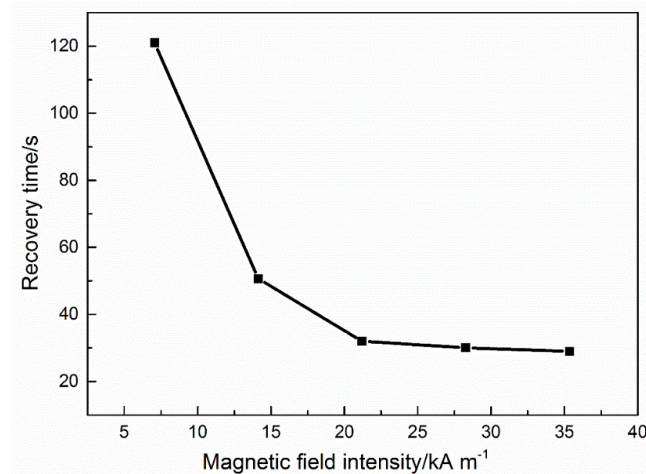


**Figure 7.** Relation between recovery time and magnetic field intensity of the 13.5 wt %  $\text{Fe}_3\text{O}_4$ /SBS/LLDPE composite.

Because of the hysteresis loss and eddy current losses in an alternating magnetic field, embedded magnetic particles in a polymer matrix will generate heat which can induce the shape memory effect [25]. A shape recovery process of 13.5 wt %  $\text{Fe}_3\text{O}_4$ /SBS/LLDPE composites is illustrated in Figure 8. The folded sample is shown as well. In the first 20 s, the sample recovery speed is low, but the shape recovery speed is very fast after 20 s. The reason is that in the first 20 s, the heat produced by  $\text{Fe}_3\text{O}_4$  nanoparticles is not enough for the temperature of the sample to reach the shape transition temperature. Thus, the internal frozen stress cannot be released to drive the shape deformation. However, when the temperature is near or higher than the shape transition temperature, the sample quickly reaches its original shape.

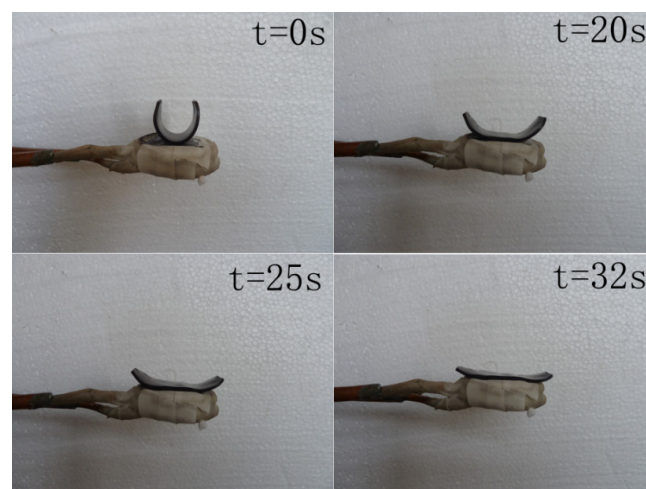


**Figure 8.** Magnetically induced shape recovery process of SBS/LLDPE composites with 13.5 wt %  $\text{Fe}_3\text{O}_4$  in an alternating field ( $f = 60 \text{ kHz}, H = 21.21 \text{ kA}\cdot\text{m}^{-1}$ ).

The shape memory properties of Fe<sub>3</sub>O<sub>4</sub>/SBS/LLDPE composites are shown in Table 1. It can be found that with increasing the content of Fe<sub>3</sub>O<sub>4</sub> nanoparticles, the shape retention rate and shape recovery rate of the composites increase significantly. In addition, the shape recovery time decreases with the increase of the Fe<sub>3</sub>O<sub>4</sub> nanoparticle content. The reason for this phenomenon is that with the increasing content of Fe<sub>3</sub>O<sub>4</sub> nanoparticles, the composites can produce more heat to let the temperature reach or near the shape transition temperature where the magnetic field response time and recovery time decrease while the shape recovery rate increases. So the recovery rate of the samples increment with Fe<sub>3</sub>O<sub>4</sub> nanoparticles content increasing [26]. It can be concluded that more nanoparticles in SBS/LLDPE blends can lead to a shorter magnetic field response time and less stress relaxation so that samples can attain a higher shape recovery rate. Furthermore, a larger Fe<sub>3</sub>O<sub>4</sub> nanoparticle content is a benefit for fixing the deformation of the composites when the temperature is near or higher than the shape transition temperature; thus the shape retention rate increases with the increase of the Fe<sub>3</sub>O<sub>4</sub> nanoparticles.

**Table 1.** Shape memory properties of the Fe<sub>3</sub>O<sub>4</sub>/SBS/LLDPE composites in an alternating magnetic field ( $f = 60$  kHz,  $H = 21.21$  kA·m<sup>-1</sup>).

Samples	$R_f$ (%)	$R_r$ (%)	Recovery Time (s)
4.5 wt % Fe <sub>3</sub> O <sub>4</sub> /SBS/LLDPE	98.5 ± 0.32	95.4 ± 0.35	118 ± 2.5
9.0 wt % Fe <sub>3</sub> O <sub>4</sub> /SBS/LLDPE	98.9 ± 0.29	97.5 ± 0.41	77 ± 1.8
13.5 wt % Fe <sub>3</sub> O <sub>4</sub> /SBS/LLDPE	99.3 ± 0.26	98.9 ± 0.42	32 ± 1.5
18.0 wt % Fe <sub>3</sub> O <sub>4</sub> /SBS/LLDPE	99.4 ± 0.28	99.0 ± 0.38	30 ± 1.6

#### 4. Conclusions

The magnetically responsive shape memory SBS/LLDPE composites with various contents of Fe<sub>3</sub>O<sub>4</sub> nanoparticles were successfully synthesized. This kind of composite exhibited excellent mechanical properties, as well as an excellent thermal-mechanical performance and shape memory behavior in an alternating magnetic field. With the increasing percentage of Fe<sub>3</sub>O<sub>4</sub> nanoparticles, the shape recovery time decreased, and the shape retention rate and shape recovery rate increased. It is expected that this demonstration will stimulate further work on the development of SMP materials for their practical applications.

**Acknowledgments:** This work was financially supported by the National Natural Science Foundation of China (Grant No. 51305320, No. 51675397 and No. 51403050), the Ningbo Natural Science Foundation (2016A610030) and the Fundamental Research Funds for the Central Universities of China (JB150408 and K5051304003).

**Author Contributions:** Yongkun Wang and Junjie Ye conceived and designed the experiments; Yongkun Wang and Wenchao Tian performed the experiments; Yongkun Wang and Junjie Ye analyzed the data; Yongkun Wang wrote the paper.

**Conflicts of Interest:** The authors declare no conflict of interest.

#### References

- Mather, P.T.; Luo, X.; Rousseau, I.A. Shape memory polymer research. *Annu. Rev. Mater. Res.* **2009**, *39*, 445–471. [[CrossRef](#)]
- Huang, W.M.; Yang, B.; An, L.; Li, C.; Chan, Y.S. Water-driven programmable polyurethane shape memory: demonstration and mechanism. *Appl. Phys. Lett.* **2005**, *86*, 114105. [[CrossRef](#)]
- Meng, H.; Li, G. A review of stimuli-responsive shape memory polymer composites. *Polymer* **2013**, *54*, 2199–2221. [[CrossRef](#)]
- Hearon, K.; Wierzbicki, M.A.; Nash, L.D.; Landsman, T.L.; Laramy, C.; Lonacker, A.T.; Gibbons, M.C.; Ur, S.; Cardinal, K.O.; Wilson, T.S. A processable shape memory polymers system for biomedical applications. *Adv. Healthc. Mater.* **2015**, *4*, 1386–1398. [[CrossRef](#)] [[PubMed](#)]
- Du, F.P.; Ye, E.Z.; Yang, W.; Shen, T.H.; Tang, C.Y.; Xie, X.L.; Zhou, X.P.; Law, W.C. Electroactive shape memory polymer based on optimized multi-walled carbon nanotubes/polyvinyl alcohol nanocomposites. *Compos. B Eng.* **2015**, *68*, 170–175. [[CrossRef](#)]

6. Jiang, Y.; Fang, L.; Kratz, K.; Lendlein, A. Influence of compression direction on the shape memory effect of micro-cylinder arrays prepared from semi-crystalline polymer networks. *MRS Adv.* **2016**, *27*, 1985–1993. [[CrossRef](#)]
7. Zhao, Q.; Marc, B.; Lendlein, A. Shape memory polymers with multiple transitions: complex actively moving polymers. *Soft Matter.* **2013**, *6*, 1744–1755. [[CrossRef](#)]
8. Zhao, Q.; Qi, H.J.; Xie, T. Recent progress in shape memory polymer: new behavior, enabling materials, and mechanistic understanding. *Prog. Polym. Sci.* **2015**, *49*, 79–120. [[CrossRef](#)]
9. Wang, Y.K.; Tian, W.C.; Xie, J.Q.; Liu, Y. Thermoelectric responsive shape memory graphene/hydro-epoxy composites for actuators. *Micromachines* **2016**, *7*, 145. [[CrossRef](#)]
10. Liu, Y.J.; Du, H.Y.; Liu, L.W.; Leng, J.S. Shape memory polymers and their composites in aerospace applications: a review. *Smart Mater. Struct.* **2014**, *23*, 023001. [[CrossRef](#)]
11. Hu, J.L.; Zhu, Y.; Huang, H.H.; Lu, J. Recent advances in shape memory polymers: Structure, mechanism, functionality, modeling and applications. *Prog. Polym. Sci.* **2012**, *37*, 1720–1763. [[CrossRef](#)]
12. Jani, J.M.; Leary, M.; Subic, A.; Gibson, M.A. A review of shape memory alloy research, applications and opportunities. *Mater. Des.* **2014**, *56*, 1079–1113.
13. Serrano, M.C.; Ameer, G.A. Recent insights into the biomedical applications of shape memory polymers. *Macromol. Biosci.* **2012**, *12*, 1156–1171. [[CrossRef](#)] [[PubMed](#)]
14. Lu, H.B.; Yao, Y.T.; Huang, W.M.; Leng, L.S.; Hui, D. Significantly improving infrared light-induced shape recovery behavior of shape memory polymeric nanocomposite via a synergistic effect of carbon nanotube and boron nitride. *Compos. B-Eng.* **2014**, *62*, 256–261. [[CrossRef](#)]
15. Wang, Y.K.; Zhu, G.M.; Xie, J.Q.; Meng, Q.N.; Liu, T.T.; Ren, F. An investigation on shape memory behavior of glass fiber/SBS/LDPE composites. *J. Polym. Res.* **2014**, *21*, 1–8. [[CrossRef](#)]
16. Zheng, N.; Fang, G.Q.; Cao, Z.L.; Zhao, Q.; Xie, T. High strain epoxy shape memory polymer. *Polym. Chem. UK* **2015**, *6*, 3046–3053. [[CrossRef](#)]
17. Yakacki, C.M.; Satarkar, N.S.; Gall, K.; Likos, R.; Hilt, J.Z. Shape memory polymer networks with Fe<sub>3</sub>O<sub>4</sub> nanoparticles for remote activation. *J. Appl. Polym. Sci.* **2009**, *112*, 3166–3176. [[CrossRef](#)]
18. Cai, Y.; Jiang, J.S.; Zheng, B.; Xie, M.R. Synthesis and properties of magnetic sensitive shape memory Fe<sub>3</sub>O<sub>4</sub>/poly( $\epsilon$ -caprolactone)-polyurethane nanocomposites. *J. Appl. Polym. Sci.* **2013**, *127*, 49–56. [[CrossRef](#)]
19. Kokate, K.K.; Bhandarkar, S.E.; Kulkarni, S.A. Synthesis And magnetic properties of poly(3,4-ethylenedioxythiophene)(PEDOT)/Fe<sub>3</sub>O<sub>4</sub> composites. *IJITR* **2015**, *3*, 1925–1929.
20. Jiao, M.; Zeng, J.; Jing, L.; Liu, C.; Gao, M. Flow synthesis of biocompatible Fe<sub>3</sub>O<sub>4</sub> nanoparticles: Insight into the effects of residence time, fluid velocity, and tube reactor dimension on particle size distribution. *Chem. Mater.* **2015**, *27*, 1299–1305. [[CrossRef](#)]
21. Pan, L.; Zhu, X.D.; Xie, X.M.; Liu, Y.T. Smart hybridization of TiO<sub>2</sub> nanorods and Fe<sub>3</sub>O<sub>4</sub> nanoparticles with pristine graphene nanosheets: Hierarchically nanoengineered ternary heterostructures for high-rate lithium storage. *Adv. Funct. Mater.* **2015**, *25*, 3341–3350. [[CrossRef](#)]
22. Hearon, K.; Smith, S.E.; Maher, C.A.; Wilson, T.S.; Maitland, D.J. The effect of free radical inhibitor on the sensitized radiation crosslinking and thermal processing stabilization of polyurethane shape memory polymers. *Radiat. Phys. Chem.* **2013**, *83*, 111–121. [[CrossRef](#)] [[PubMed](#)]
23. Liu, Y.Y.; Han, C.M.; Tan, H.F.; Du, X.W. Thermal, mechanical and shape memory properties of shape memory epoxy resin. *Mat. Sci. Eng. A Struct.* **2010**, *527*, 2510–2514. [[CrossRef](#)]
24. Wang, Y.K.; Zhu, G.M.; Cui, X.P.; Liu, T.T.; Liu, Z.; Wang, K. Electroactive shape memory effect of radiation cross-linked SBS/LLDPE composites filled with carbon black. *Colloid Polym. Sci.* **2014**, *292*, 2311–2317. [[CrossRef](#)]
25. Mohammadi, A.; Barikani, M.; Barmar, M. Synthesis and investigation of thermal and mechanical properties of in situ prepared biocompatible Fe<sub>3</sub>O<sub>4</sub>/polyurethane elastomer nanocomposites. *Polym. Bull.* **2015**, *72*, 219–234. [[CrossRef](#)]
26. Razzaq, M.Y.; Anhalt, M.; Frommann, L.; Weidenfeller, B. Thermal, electrical and magnetic studies of magnetite filled polyurethane shape memory polymers. *Mater. Sci. Eng. A Struct.* **2007**, *444*, 227–235. [[CrossRef](#)]

